

Provided for non-commercial research and education use.
Not for reproduction, distribution or commercial use.



(This is a sample cover image for this issue. The actual cover is not yet available at this time.)

This article appeared in a journal published by Elsevier. The attached copy is furnished to the author for internal non-commercial research and education use, including for instruction at the author's institution and sharing with colleagues.

Other uses, including reproduction and distribution, or selling or licensing copies, or posting to personal, institutional or third party websites are prohibited.

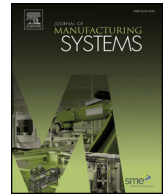
In most cases authors are permitted to post their version of the article (e.g. in Word or Tex form) to their personal website or institutional repository. Authors requiring further information regarding Elsevier's archiving and manuscript policies are encouraged to visit:

<http://www.elsevier.com/authorsrights>



Contents lists available at ScienceDirect

Journal of Manufacturing Systems

journal homepage: www.elsevier.com/locate/jmansys

High definition metrology enabled three dimensional discontinuous surface filtering by extended tetrolet transform

Yiping Shao^a, Kun Wang^a, Shichang Du^{a,b,*}, Lifeng Xi^{a,b}^a School of Mechanical Engineering, Shanghai Jiao Tong University, No. 800 Dongchuan Road, Shanghai, 200240, China^b State Key Lab of Mechanical System and Vibration, Shanghai Jiao Tong University, Shanghai, 200240, China

ARTICLE INFO

Keywords:

3D discontinuous surface
 Extended tetrolet transform
 Surface quality
 Filtering
 High definition metrology

ABSTRACT

Surface topography is of great importance for the functional behavior of a part, and filtering is a key step in achieving topography analysis. The traditional filtering methods such as Gaussian and spline filter have been effectively applied in the continuous surface, but most parts have a great quantity of crucial discontinuous surfaces in engineering practice. A new filtering method based on extended tetrolet transform is proposed for the three dimensional (3D) discontinuous surface in this paper. The proposed filtering method consists of 3D discontinuous surface measurement and point cloud conversion, edge detector generation, extended tetrolet transform and 3D characterization parameters evaluation. It overcomes the drawback of edge effect which occurs in the discontinuous surface using traditional filtering methods. The 3D discontinuous surface is measured by high definition metrology that can generate millions of data points representing the entire surface. To verify the effectiveness of the extended tetrolet transform, it is compared with the areal Gaussian filter and areal spline filter both for the simulated continuous and discontinuous surface. The low frequency and high frequency components of engineering surfaces are separated exactly, and these results demonstrate that the proposed method is effective for the 3D discontinuous surface filtering without edge distortions.

1. Introduction

Over the past 30 years, there has been an increasing interest in the relationship between surface topography and mechanical manufacturing. Surface topography is a vital link between a part generated by manufacturing process and the functionality that is expected of it [1]. To satisfy tighter tolerances and higher performance standards, there is a need for engineers to go beyond specifying sizes, shapes, and peaks and move toward specifications of various surface functional attributes. Surface can be considered as the linear superposition of flaws, form error and surface texture which contains waviness and roughness [2]. Moreover, surface can be separated into different frequency components from smaller scale to larger scale, such as roughness, waviness, and form. This separation scheme had been recognized from surface texture measurement at the early stage. The motivation for such classification comes from the fact that these surface features in different scales have different origins and affect part functionality in different ways. They can be used to reflect different functions of workpieces, such as vibration, tool wear, chatter and seal [3–5]. Malburg et al. presented a novel method for the analysis of surface profiles in contact with comfortable properties of components such as gaskets,

seals and bushings in many engine and hydraulic applications [6]. Bottiglione et al. [7,8] proposed a method where surface topography parameters, the applied load and the geometry of the seal were the major factors which affected leakage mechanism contained leak path formation and leakage calculation.

Surface filtering is a process to partition a surface profile into form, waviness and roughness, which is a crucial aspect of surface topography analysis. Up to now, surface filtering has been widely employed in surface metrology and a relatively mature system has been developed. An areal spline filtering technique has been proposed for 3D surface in these studies [9,10]. Wavelet transform was adopted to engineering surface texture analysis and different wavelet bases were compared by Fu et al. [11]. The applicability of wavelets was highlighted through the multi-resolution analysis on surface profiles. Jiang et al. [12] proposed a lifting wavelet representation for characterization of surface topography. Raja et al. reviewed the common filter techniques which contained traditional methods and advanced methods, such as 2RC, Gaussian, spline, morphological, wavelet, regression filters and robust regression filters [13].

Most surface filtering researches concentrate on the continuous surface, but it exists a great quantity of crucial discontinuous surfaces in

* Corresponding author at: School of Mechanical Engineering, Shanghai Jiao Tong University, No. 800 Dongchuan Road, Shanghai, 200240, China.

E-mail addresses: syp123gh@sjtu.edu.cn (Y. Shao), wangkun1224@sjtu.edu.cn (K. Wang), lovbin@sjtu.edu.cn (S. Du), lfxi@sjtu.edu.cn (L. Xi).

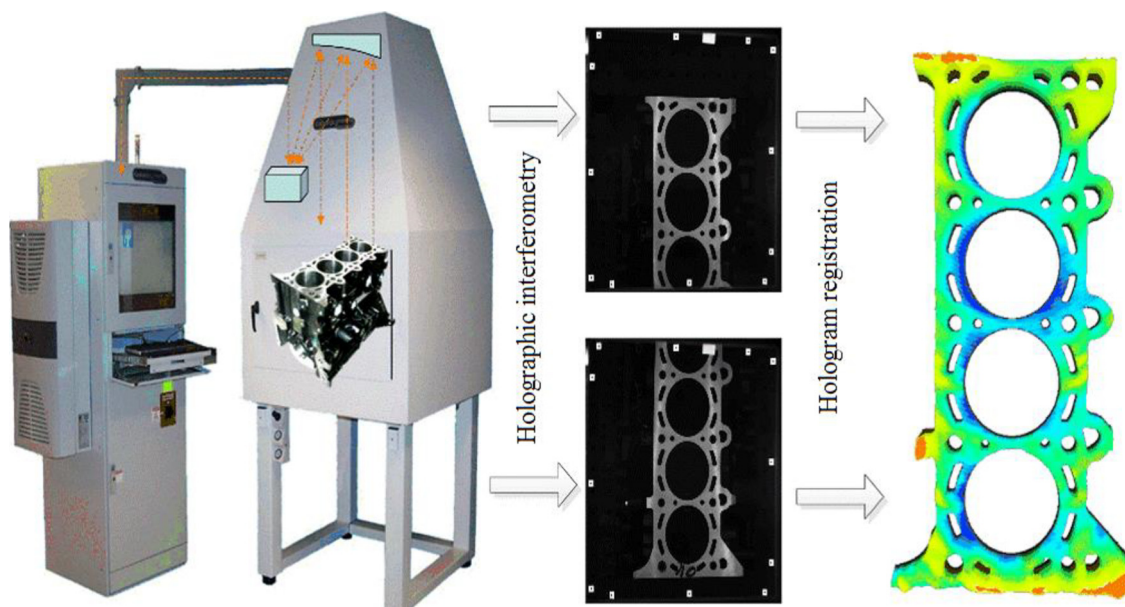


Fig. 1. Measurement by HDM.

engineering practice, such as engine block faces with cylinder holes, bolt holes and cooling holes. Conventionally, most surfaces are measured by the widely-used coordinate measuring machine (CMM). However, with the low-density sampling, the measurement result of CMM cannot represent the entire surface topography. Therefore, a full-inspection and high-density sampling measuring instrument is necessary for large and discontinuous surfaces. Recently, a novel measuring instrument called non-contact high definition metrology (HDM) has been developed [14]. Coherix ShaPix (ShaPix® Surface Detective™, Ann Arbor, MI) is the device for HDM measuring process. It is a new laser holographic interferometry measurement that can measure entire surface height of discontinuous objects with holes and empty zones instead of a local area. Millions of data points are generated on an area of $300\text{ mm} \times 300\text{ mm}$ within seconds to represent the entire measured surface with $150\text{ }\mu\text{m}$ lateral resolution in x - y direction and $1\text{ }\mu\text{m}$ accuracy in z direction. Fig. 1 shows the HDM device and a measured engine block face. Based on HDM, some researches such as 3D surface topography evaluation [15], filtering [16,17], classification [18,19], forecasting [20] and monitoring methods [21–24] have been developed for the pre-control of the manufacturing process.

However, few filtering researches had been conducted on the discontinuous surface using HDM. Zhang et al. [25] utilized a Gaussian (DoGs) filter bank to achieve the classification of workpiece surface by extracting features from HDM data. Liao et al. [26] presented a method of utilizing biorthogonal wavelets to decompose 3D surface into multi-scale subsurface and also demonstrated the relationship between wavelet scale and surface features. For the discontinuous surface, edge distortion is usually caused by holes and boundaries in the surface. To be specific, edge distortion is the pattern of manifestation of the singularity. The edge distortion belongs to the point singularity in the two dimensional discontinuous surface, and it is corresponding to the line and surface singularities in the three dimensional discontinuous surface. The discrete wavelet transform (DWT) has been one of the most popular tools in image processing due to its promising properties for point singularity analysis that can solve edge distortion. But the DWT fails to achieve geometric features with line and surface singularities, and its basis functions are fixed on the horizontal, vertical and diagonal directions without adapting the image geometric structures. Therefore, it is necessary to develop an optimal filtering technique for the 3D discontinuous surface.

A latest academic discipline called multi-scale geometric analysis

(MGA) has been developed in harmonic analysis. The major goal of MGA is to explore the optimal representation of high dimensional data, and it can be extended to surface filtering. Tetrolet transform is the latest MGA method, which is a non-redundant adaptive geometric wavelet transform [27,28]. Due to small support, symmetry and orthogonality, tetrolet does not suffer from pseudo-Gibbs artifacts while preserving the anisotropic edges and features. It provides a simple but enormously fast and effective approach for image processing and compression of real data arrays. However, the standard tetrolet transform can represent the original surface well, but it lacks the representation for the decomposed and reconstructed subsurface. In order to adapt to the discontinuous surface filtering, the tetrolet transform need to be extended. Therefore, the limitations of current methods are summarized as follows:

- Surface topography directly related to mechanical properties and functional attributes, and different surface components reflect different functions of workpieces, such as vibration, tool wear, chatter and seal [3–5].
- Filtering is a key step to extract surface components. Traditional filtering methods such as Gaussian and spline filter are only appropriate for continuous surfaces, they cannot be used for discontinuous surfaces due to boundary distortion or end effects problems.
- Many discontinuous surfaces exist in engineering practice, such as the engine block faces, the engine desk faces and automatic transmission valve joint surfaces. It is necessary to propose a filtering method for discontinuous surfaces.

Meanwhile, to the best knowledge of the authors, there is no tetrolet transform based filtering method for the discontinuous surface using HDM. Benefiting from the development of measurement, the main contribution of this paper is to present a novel filtering method for the discontinuous surface based on extended tetrolet transform. The proposed filtering method overcomes the drawback of edge effect which occurs in the discontinuous surface using traditional filtering methods. The low frequency and high frequency components of discontinuous engineering surfaces are separated exactly without edge distortions. Once the exact surface components are obtained, they can indicate the machining process and the function of the part properly.

The paper is organized as follows: The basic idea of tetrolet

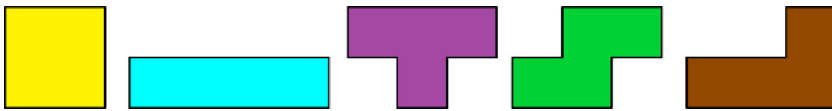


Fig. 2. The five free tetrominoes.

transform is briefly introduced in Section 2. In Section 3, the proposed filtering method for the discontinuous surface is described. Then, in the next section, a detailed description of numerical simulation for the continuous and discontinuous surface is given to validate feasibility of the presented method. Section 5 gives two specific case studies for verifying the proposed method in engineering applications. Then, a further discussion of the proposed method is described in Section 6. Finally, the last section draws the conclusions.

2. Brief introduction of tetralet transform

Tetralet transform is based on the concept of tetrominoes which was proposed by Golomb [29]. They are different forms made by a union of four unit squares. Each square is connected to at least one other square along an edge. There are five kinds of tetrominoes in different forms without rotations and reflections, which are so-called free tetrominoes (see Fig. 2). It is clear that any image of size $N \times N$ (N is even) could be made up of basic tetrominoes. Especially, there are 117 solutions for covering of a 4×4 board with tetrominoes.

The basic idea of tetralet is similar to wedgelet, where Haar functions are applied on the edge parts. For an image $\mathbf{a} = (a[m_1, m_2])_{(m_1, m_2) \in I}$ with $I = \{0, \dots, N-1\} \subset \mathbb{Z}^2$, $N = 2^J$, $J \in \mathbb{N}$, it can be divided into a series of 4×4 blocks. The four tetrominoes in a 4×4 block are denoted by $\{I_0, I_1, I_2, I_3\}$ and the four indices in each subsets I_v are mapped to a the scalar set $\{0, 1, 2, 3\}$ by a bijective mapping L . For any tetromino I_v , the discrete basis functions are defined as:

$$\phi_{I_v}[m_1, m_2] := \begin{cases} 1/2(m_1, m_2) \in I_v \\ 0 \text{ otherwise} \end{cases} \quad (1)$$

and

$$\psi_{I_v}^l[m_1, m_2] := \begin{cases} \varepsilon[l, L(m_1, m_2)] & (m_1, m_2) \in I_v \\ 0 & \text{otherwise} \end{cases} \quad (2)$$

for $l = 1, 2, 3$. Due to the underlying tetromino support, $\psi_{I_v}^l$ are called tetralets and ϕ_{I_v} is the corresponding scaling function. In the tetralet definition, the function values $\varepsilon[l, L(m_1, m_2)]$ entries from Haar wavelet transform matrix

$$W := (\varepsilon[l, m])_{l, m=0}^3 = \frac{1}{2} \begin{pmatrix} 1 & 1 & 1 & 1 \\ 1 & 1 & -1 & -1 \\ 1 & -1 & 1 & -1 \\ 1 & -1 & -1 & 1 \end{pmatrix} \quad (3)$$

Analogous to wavelet transform, tetralet transform decomposes an image into the low frequency coefficients and high frequency tetralet coefficients at the specified level. The major difference is that tetralet transform divides the original image into blocks of size 4×4 and chooses the optimal tetromino partition which is adapted to the image geometry in the block among the 117 solutions [27]. A k levels decomposition procedures of the tetralet transform are summarized as follows:

Step 1: The original image is divided into 4×4 blocks. Each block is covered with any four free tetrominoes.

Step 2: Based on the principle of the sparsest tetralet representation, the optimal covering is found in each block among the 117 solutions.

Step 3: According to the number of the deviations, the low frequency coefficients and high frequency tetralet coefficients of each block are rearranged into a 2×2 block.

Step 4: The low frequency coefficients and high frequency tetralet coefficients are stored.

Step 5: Apply steps 1–4 to the low frequency coefficients for the next decomposition until the level k .

After a proper decomposition, the low frequency coefficients and high frequency tetralet coefficients of the original image in each level can be obtained.

3. The proposed method

3.1. Overview of the proposed method

This section proposes a novel filtering method for the discontinuous surface based on extended tetralet transform. Comparing with the traditional methods, three aspects are improved: 1) Due to small support, symmetry, orthogonality and adaptive geometrical structure, the proposed method can solve the line and surface singularities in the 3D discontinuous surface which causes edge distortions. 2) The proposed method develops an edge detector to identify the surface boundaries and holes in advance so that different forms of decomposition are applied. 3) The proposed method can well extract the decomposed and reconstructed subsurface which represent different surface components. The proposed method consists of 3D discontinuous surface measurement and point cloud conversion, edge detector generation, extended tetralet transform and 3D characterization parameters evaluation. The framework is shown in Fig. 3. The procedure involves the following steps.

Step 1: HDM is employed to measure the 3D discontinuous surface and generate millions of points. A converted gray image which can represent the entire surface is gained by the point cloud [15].

Step 2: Edge detector generation. An edge detector is generated to detect the boundaries and holes of the discontinuous surface in advance. As for the edge and no edge, different forms of decomposition are applied, which are used to avoid end effects.

Step 3: Extended tetralet transform. The extended tetralet transform is divided into three modules: decomposition, shrinkage and reconstruction. Once the decomposed and reconstructed subsurface are obtained by the extended tetralet transform, a relationship between the decomposition level and the actual surface components is built. Based on the relationship, the discontinuous surface is separated into the surface form and waviness exactly.

Step 4: 3D characterization parameters evaluation. The latest 3D characterization parameters including height parameters, shape parameters and spatial parameters are calculated to evaluate the filtered surface components for surface topography analysis.

3.2. Surface measurement and point cloud conversion

To get the real surface information, all the surfaces are measured by high definition metrology which provides a good platform to analyze the surface topography. Due to the precision measurement, millions of data points are generated by Shapix to represent the measured surface. A preprocessing method to convert the mass data points into a height-encoded and position-maintained gray image is proposed by Wang et al. [15]. The method has provided many advantages for the next step. The lower and upper specification S_L and S_U in Z direction are assigned from $-30 \mu\text{m}$ to $30 \mu\text{m}$. Due to the lateral resolution, HDM cannot measure roughness, and the HDM data only contains the 3D surface form and waviness information. Two measured examples of the engine cylinder block surface and head surface are shown in Fig. 4.

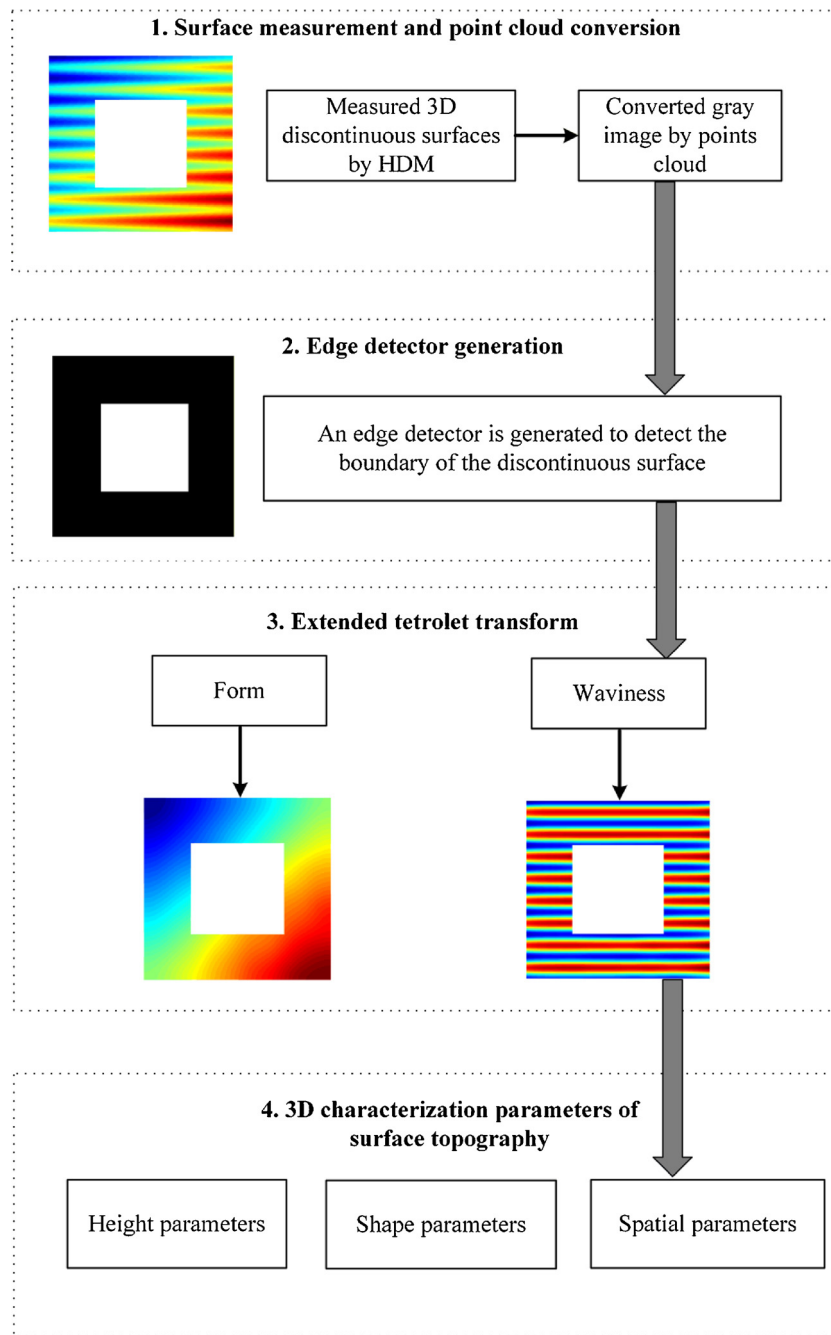


Fig. 3. The framework of the proposed method.

3.3. An edge detector for the discontinuous surface

The major difference between the filtering of discontinuous surfaces and continuous surfaces is that the surface boundary of the former is already known in advance. To achieve the filtering in the discontinuous surface without any distortions, an edge detector w is developed to identify the surface boundary. As for the edge and no edge, different forms of decomposition in the extended tetrolet transform are applied, which are used to avoid end effects. An architecture of the developed algorithm is shown in Fig. 5 and the detailed procedures are described as follows.

Step 1: Convolution operation

For a discontinuous surface $a = [a(m_1, m_2)]_{m_1, m_2=0}^{N-1}$ can be represented by a matrix of size $N \times N$, the convolution sum b is calculated as:

$$b = a * h_1 + a * h_2 \quad (4)$$

where the symbol $*$ means convolution operation, b has the same sizes with a . The convolution kernels h_1 and h_2 are defined as:

$$h_1 = (1 \ -1), \quad h_2 = (1 \ -1)^T \quad (5)$$

The boundaries and holes in the surface are crucial positions where the pixel size changes rapidly, and these pixels are called singular points. The convolution operation aims to find singular points in the surface by traversing the entire surface. According to the distribution of singular points, the boundaries and holes are obvious.

Step 2: Cycle Spinning

The convolution sum b is also a matrix of size $N \times N$, let the elements of the N th column and the N th row of the matrix b be equal to 0. The new matrix g_0 is defined as:

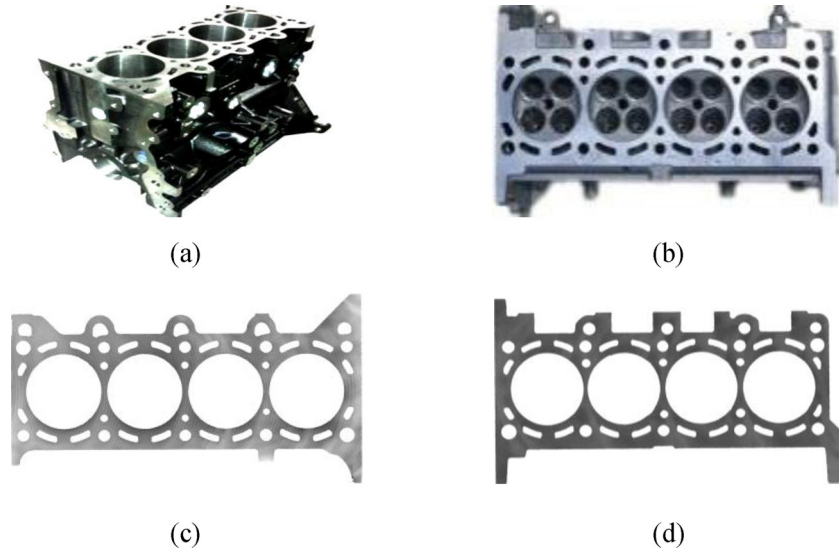


Fig. 4. (a) Engine cylinder block surface (b) Engine cylinder head surface (c) The converted gray image of the block surface (d) The converted gray image of the head surface.

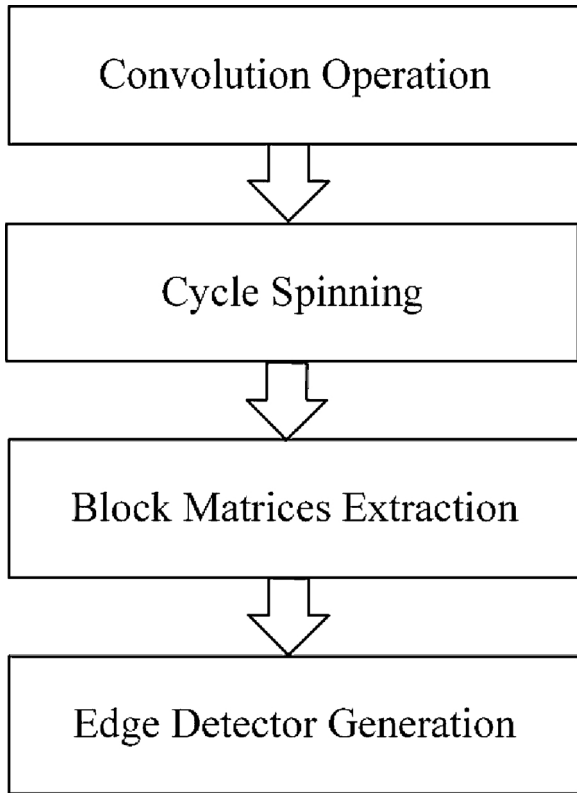


Fig. 5. The architecture of the developed algorithm.

$$\mathbf{g}_0 = \begin{pmatrix} (\mathbf{B}_1)_{(N-1) \times (N-1)} & \mathbf{0}_{(N-1) \times 1} \\ \mathbf{0}_{1 \times (N-1)} & \mathbf{0}_{1 \times 1} \end{pmatrix} \quad (6)$$

When the boundaries and holes are found, cycle spinning is applied to compensate for the lack of translation invariance property and suppress pseudo-Gibbs phenomena of the surface. The purpose of cycle spinning is to smooth the surface and decrease the distortion. To be specific, it changes the order of surface pixels, thereby changing the position of singular points in the entire surface to reduce the amplitude of the oscillation. The operator of cycle spinning $CS_{p,q}$ is defined as:

$$CS_{p,q}(g_0(m_1, m_2)) = g_0(\text{mod}(m_1 + p, N), \text{mod}(m_2 + q, N)) \quad (7)$$

where p, q are the numbers of shifts in column and row respectively. Then the updated matrix \mathbf{g} is defined as:

$$\mathbf{g} = CS_{0,-1}(CS_{-1,0}(\mathbf{g}_0)) \quad (8)$$

Step 3: Block Matrices Extraction

Following the steps above, the size of processed surface is equal to the original surface, which doesn't match the block $sN_{u_0} \times N_{u_0}$ structure of tetrolet transform. In order to adapt to the 4×4 block in tetrolet transform, the processed surface should be reduced by 4 times both in the x and y directions by taking one of four points. Therefore, the updated matrix \mathbf{g} is separated into block matrices. A new matrix \mathbf{u}_0 is calculated as:

$$\mathbf{u}_0 = \mathbf{g} * \mathbf{K}_4 \quad (9)$$

where \mathbf{K}_4 is a matrix of size 4×4 and the size of \mathbf{u}_0 depends on $\mathbf{g} \cap \mathbf{K}_4$, $N_{u_0} = N - 4 + 1 = N - 3$. The matrix \mathbf{K}_4 is given as:

$$\mathbf{K}_4 = \begin{pmatrix} 1 & 1 & 1 & 1 \\ 1 & 1 & 1 & 1 \\ 1 & 1 & 1 & 1 \\ 1 & 1 & 1 & 1 \end{pmatrix} \quad (10)$$

Let $\mathbf{u}_0 = \{u_0(i, j), i = 0, \dots, N_{u_0} - 1, j = 0, \dots, N_{u_0} - 1\}$, the extracted block matrix \mathbf{u} is defined as:

$$\mathbf{u} = \{u(i', j'), i' = 0, \dots, N_u - 1, j' = 0, \dots, N_u - 1\} \quad (11)$$

where $u(i', j') = u_0(4i', 4j')$ and $N_u = \lfloor (N_{u_0} - 1)/4 \rfloor$

Step 4: Edge Detector Generation

This step is to determine the value of the edge detector by the certain threshold. Generally, the threshold is given by the advanced information of the original surface. Let \mathbf{w} be the edge detector of the surface \mathbf{a} , it is defined as:

$$\mathbf{w} = \{w(i', j'), i' = 0, \dots, N_u - 1, j' = 0, \dots, N_u - 1\} \quad (12)$$

$$w(i', j') = \begin{cases} 0, & |u[i', j']| > \theta \\ 1, & |u[i', j']| \leq \theta \end{cases} \quad (13)$$

where θ is the threshold to determine whether the pix point belongs to the surface or not. If the pix point belongs to the surface, $w(i', j') = 0$, otherwise $w(i', j') = 1$.

Example 1. Consider a selected part of a discontinuous surface which is shown in Fig. 6, the corresponding edge detector \mathbf{w} is generated through the above algorithm ($\theta = 0$). It is clear that the surface boundary is well identified.

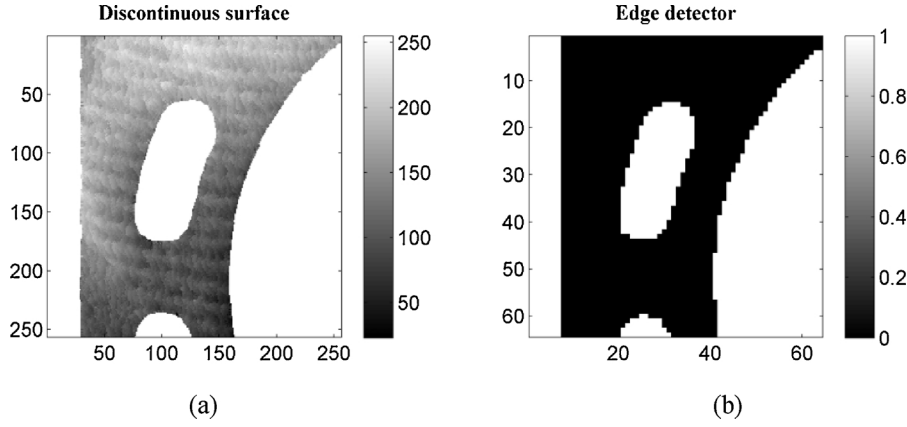


Fig. 6. (a) A discontinuous surface (b) The edge detector.

3.4. Extended tetrolet transform

3.4.1. The idea of the extended tetrolet transform

A wavelet based filtering method of engineering surface has been accepted by ISO 16610-29 [30]. As a non-redundant adaptive geometric wavelet transform, tetrolet transform has the similar property. In the tetrolet transform, an original surface \mathbf{a} can be decomposed into the low-pass approximation parts (low frequency coefficients) a_i and the high-pass multiscale detail parts (high frequency tetrolet coefficients) d_i . Let a_0 denotes the original surface, a logical tetrolet decomposition equation in J levels is listed below:

$$\begin{aligned} a_0 &= a_1 + d_1 \\ &= a_2 + d_2 + d_1 \\ &= a_3 + d_3 + d_2 + d_1 \\ &= \dots \\ &= a_j + d_j + d_{j-1} + \dots + d_1 \end{aligned} \quad (14)$$

Accordingly, the multiresolution form of the tetrolet transform consists of constructing a ladder of approximations to the surface. The specific procedures are illustrated in Fig. 7.

Reversing the ladder structure, the i th subsurface M_i can be reconstructed from the reconstructed low frequency coefficients \tilde{a}_i and the reconstructed high frequency tetrolet coefficients \tilde{d}_i . Therefore, the i th subsurface M_i is defined as:

$$M_i = \tilde{a}_i + \tilde{d}_i \quad (15)$$

As mentioned above, the standard tetrolet transform lacks the representation for the decomposed and reconstructed subsurface. The down-sampling process in the decomposition makes the size of the low frequency coefficients and high frequency tetrolet coefficients half the size of the previous low frequency coefficients, therefore the subsurface cannot be the same size as the original surface. To achieve the discontinuous surface filtering, the tetrolet transform is extended. The extended tetrolet transform is divided into three modules: decomposition, shrinkage and reconstruction. The flow chart of the extended tetrolet transform algorithm is illustrated in Fig. 8, and the detailed procedures are explained as follows.

Module 1: Decomposition

For a discontinuous surface $\mathbf{a} = [a(m_1, m_2)]_{m_1, m_2=0}^{N-1}$, r levels decomposition is implemented. The decomposition logic is also suitable for the extended tetrolet transform, and the low-pass approximation part

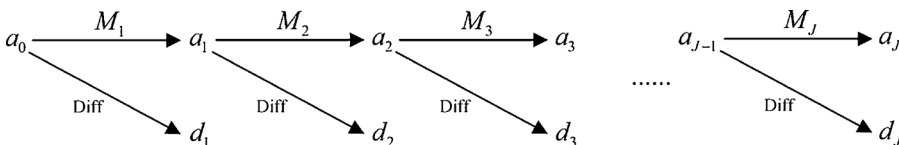


Fig. 7. A multiresolution separation using the extended tetrolet transform.

$a_{r-1}[m_1, m_2]$ can be decomposed as:

$$\begin{aligned} a_{r-1}[m_1, m_2] &= \sum_{l=1}^3 \sum_{v=0}^3 d_r^l[m_1, m_2] \psi_v^l[m_1, m_2] \\ &+ \sum_{v=0}^3 a_r[m_1, m_2] \phi_{I_v}[m_1, m_2] \end{aligned} \quad (16)$$

where $I = \{I_v | v = 0, 1, 2, 3\} = \{(m_1, m_2) : m_1, m_2 = 0, \dots, N-1\} \subset \mathbb{Z}^2$, $r = 1, 2, \dots, J-1, N = 2^J, J \in \mathbb{N}$.

Step 1: In the r th level, the low-pass approximation part a_{r-1} is divided into blocks Q of size 4×4 .

Step 2: Each block Q has 117 tetromino tilings $k = 1, \dots, 117$. The tetromino subsets ($v = 0, 1, 2, 3$) is ordered by the pixel size, and the corresponding mapping $L(m', n') = \{0, 1, 2, 3\}$, $m', n' \in I_v^{(k)}$.

(a) If the edge detector $w(i', j') = 0$, the pix point belongs to the surface and this is not the edge. Haar wavelet transform is applied in each tiling k and the low frequency coefficients $a_r^{(k)}$ and high frequency tetrolet coefficients $d_r^{l(k)}$ with $l = 1, 2, 3$ are obtained as follows:

$$a_r^{(k)} = a_r^{(k)}[v]_{v=0}^3 \text{ with } a_r^{(k)}[v] = \sum_{(m', n') \in I_v^{(k)}} \varepsilon[0, L(m', n')] a_{r-1}[m', n'] \quad (17)$$

$$d_r^{l(k)} = d_r^{l(k)}[v]_{v=0}^3 \text{ with } d_r^{l(k)}[v] = \sum_{(m', n') \in I_v^{(k)}} \varepsilon[l, L(m', n')] a_{r-1}[m', n'] \quad (18)$$

According to the rule of minimal norm which satisfies:

$$k^* = \arg \min \sum_{l=1}^3 \sum_{v=0}^3 |d_r^{l(k^*)}[v]| \quad (19)$$

the optimal low frequency coefficients and high frequency tetrolet coefficients $[a_r^{(k^*)}, d_r^{1(k^*)}, d_r^{2(k^*)}, d_r^{3(k^*)}]$ are found.

(b) If the edge detector $w(i', j') = 1$, the pix point doesn't belong to the surface and this is the edge. The block Q satisfies the tetromino tiling $k = 1$. The low frequency coefficients $a_r^{(k)}$ and high frequency tetrolet coefficients $d_r^{l(k)}$ with $l = 1, 2, 3$ are calculated by the specified Haar wavelet transform matrix $\mathbf{h}\mathbf{a}$:

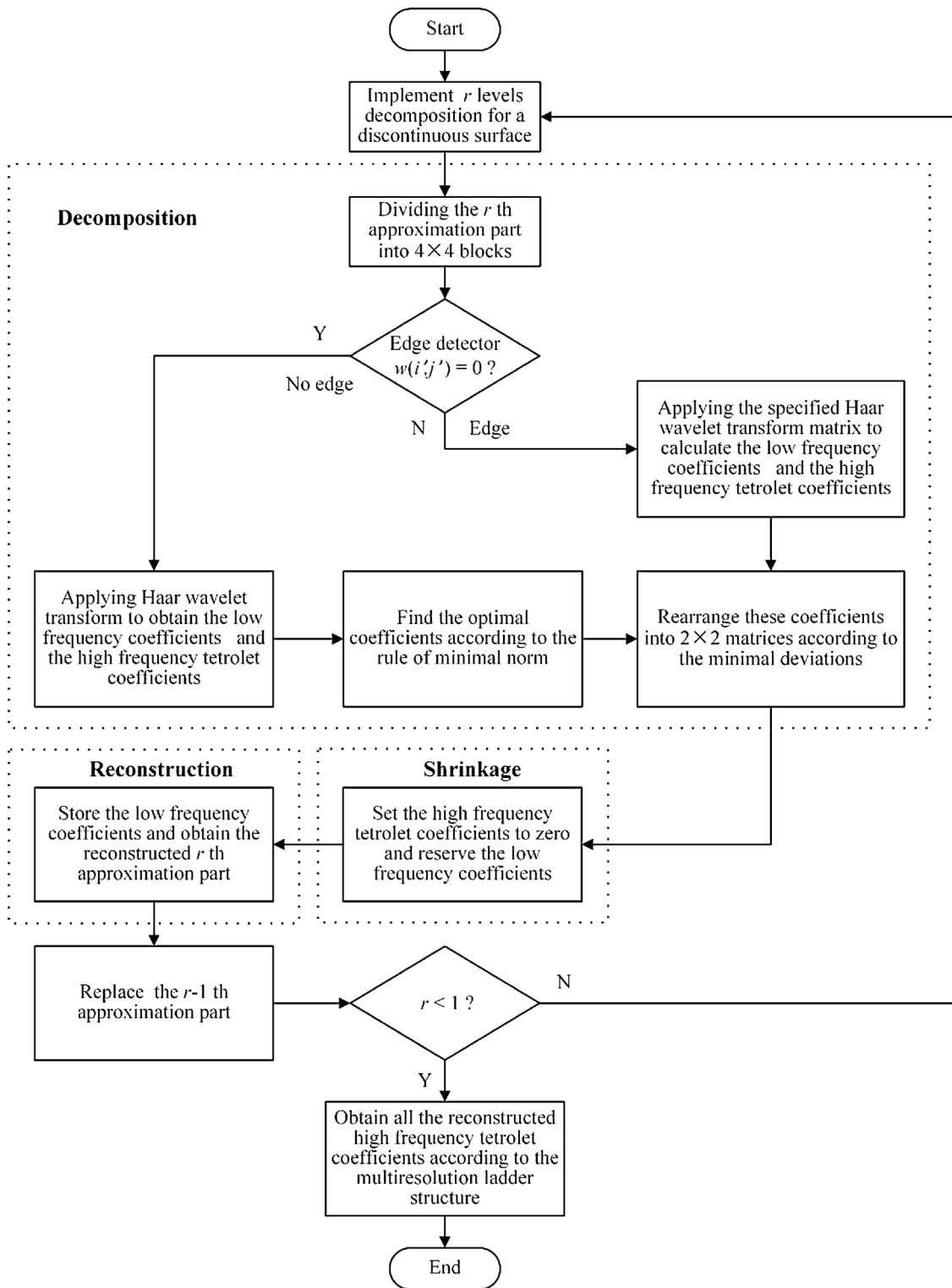


Fig. 8. Extended tetrolet transform algorithm.

$$\mathbf{ha} = \begin{pmatrix} \mathbf{ha}_1 & \mathbf{ha}_2 & \mathbf{0} & \mathbf{0} \\ \mathbf{ha}_3 & \mathbf{ha}_4 & \mathbf{0} & \mathbf{0} \\ \mathbf{0} & \mathbf{0} & \mathbf{ha}_1 & \mathbf{ha}_2 \\ \mathbf{0} & \mathbf{0} & \mathbf{ha}_3 & \mathbf{ha}_4 \end{pmatrix} = \{ha_{ij} \mid i, j = 1, 2, \dots, 16\} \quad (20)$$

$$a_r^{(k)} = \left\{ \sum_{j=1}^{16} ha_{ij} \times a_{r-1}[m', n'] \mid i = 1, 5, 9, 13 \right\} \quad (21)$$

$$d_r^{l(k)} = \left\{ \sum_{j=1}^{16} ha_{ij} \times a_{r-1}[m', n'] \mid i = 2, 3, 4, 6, 7, 8, 10, 11, 12, 14, 15, 16 \right\} \quad (22)$$

where $\mathbf{ha}_1 = \frac{1}{2} \begin{pmatrix} 1 & 1 & 0 & 0 \\ 1 & 1 & 0 & 0 \\ 1 & -1 & 0 & 0 \\ 1 & -1 & 0 & 0 \end{pmatrix}$, $\mathbf{ha}_2 = \frac{1}{2} \begin{pmatrix} 1 & 1 & 0 & 0 \\ -1 & -1 & 0 & 0 \\ 1 & -1 & 0 & 0 \\ -1 & 1 & 0 & 0 \end{pmatrix}$, \mathbf{h}

$$\mathbf{a}_3 = \frac{1}{2} \begin{pmatrix} 0 & 0 & 1 & 1 \\ 0 & 0 & 1 & 1 \\ 0 & 0 & 1 & -1 \\ 0 & 0 & 1 & -1 \end{pmatrix} \text{ and } \mathbf{ha}_4 = \frac{1}{2} \begin{pmatrix} 0 & 0 & 1 & 1 \\ 0 & 0 & -1 & -1 \\ 0 & 0 & 1 & -1 \\ 0 & 0 & -1 & 1 \end{pmatrix}.$$

Step 4: Compute the number of deviations from the tiling, rearrange the optimal low frequency coefficients $a_r^{(k^*)}$ and high frequency tetralet coefficients $d_r^{l(k^*)}$ into a 2×2 matrix according to the minimal deviations.

i.e. $a_r = \mathbf{R}(a_r^{(k^*)}) = \begin{bmatrix} a_r^{(k^*)}[0], a_r^{(k^*)}[2] \\ a_r^{(k^*)}[1], a_r^{(k^*)}[3] \end{bmatrix}$ and $d_r^l = \mathbf{R}(d_r^{l(k^*)}) = \begin{bmatrix} d_r^{l(k^*)}[0], d_r^{l(k^*)}[2] \\ d_r^{l(k^*)}[1], d_r^{l(k^*)}[3] \end{bmatrix}$

Module 2: Shrinkage

After a proper decomposition, a shrinkage procedure is applied to these coefficients. As an acknowledged approach, the global hard threshold function $S_\alpha(x)$ is used in the extended tetralet transform. The threshold parameter α depends on the certain number of largest tetralet coefficients which is retained.

Step 5: Set the high frequency tetralet coefficients to zero and reverse the low frequency coefficients. The specific function is listed below:

$$S_\alpha(d_r^{l(k^*)}) = \begin{cases} d_r^{l(k^*)}, & |d_r^{l(k^*)}| \geq \alpha \\ 0, & |d_r^{l(k^*)}| < \alpha \end{cases} \quad (23)$$

where $\alpha = M$ and M is a very big positive constant which is bigger than all the absolute value of the high frequency tetralet coefficients.

Module 3: Reconstruction

In order to keep the approximation part the same size as the original surface a , the r th approximation part a_r needed to be reconstructed. The process of the coefficients' recombination can be called inverse extended tetralet transform.

Step 6: The reconstructed equation is listed below:

$$\begin{aligned} \tilde{a}_r[m_1, m_2] &= \sum_{l=1}^3 \sum_{v=0}^3 S_\alpha(d_r^l[m_1, m_2]) \psi_{lv}^l[m_1, m_2] \\ &+ \sum_{v=0}^3 a_r[m_1, m_2] \phi_{lv}[m_1, m_2] \end{aligned} \quad (24)$$

where $I = \{I_v \mid v = 0, 1, 2, 3\} = \{(m_1, m_2) : m_1, m_2 = 0, \dots, N-1\} \subset \mathbb{Z}^2$, $N = 2^J$, $J \in \mathbb{N}$.

Step 7: Store the reconstructed \tilde{a}_r , and replace the low-pass approximation part a_{r-1} by a_{r-2} until $r < 1$.

Step 8: Obtain all the reconstructed high frequency tetralet coefficients \tilde{d}_r^l according to the multiresolution ladder structure, such as $\tilde{d}_r^l = \tilde{a}_{r-1} - \tilde{a}_r$.

3.4.2. Transformation between decomposition levels and surface components

Surface filtering mainly concerns the separation of topographical components. These components are usually characterized by wavelength or frequency, as designated in the terms of form, waviness and roughness. In fact, form consists of all low frequency components, and waviness and roughness are collections of high frequency or small-wavelength for every engineering surface. So the surface can be divided into two parts with low-pass and high-pass.

Example 2. A 3D engineering surface:

$$S(x, y) = L(x, y) + H(x, y) \quad (25)$$

where $L(x, y)$ is the low-pass part which represents the form components, and $H(x, y)$ is the high-pass part which represents the waviness and roughness components. It is clear that it has $L(x, y) = F(x, y)$ and $H(x, y) = W(x, y) + R(x, y)$, where $F(x, y)$ is the form, $W(x, y)$ is the waviness and $R(x, y)$ is the roughness.

As the HDM data only contains the 3D surface form and waviness information, the original surface satisfies the following convention in this paper:

$$\begin{aligned} S(x, y) &= L(x, y) + H(x, y) \\ &= F(x, y) + W(x, y) \end{aligned} \quad (26)$$

To clarify the general sense of the surface components at each decomposition level, there is a need to build a connection between the decomposition level and the actual surface components. Analogous to "transmission bandwidth", a surface variable M_{ij} is constructed by calculating the difference between the i th subsurface M_i and the j th subsurface M_j .

$$\begin{aligned} M_{i,j} &= M_i - M_j \\ &= \tilde{a}_i + \tilde{a}_i - \tilde{a}_j - \tilde{a}_j \\ &= \tilde{a}_{j-1} + \tilde{a}_{j-2} + \dots + \tilde{a}_i \quad (i < j) \end{aligned} \quad (27)$$

where the level i is corresponding to the cutoff wavelength λ_i , and the level j is corresponding to the cutoff wavelength λ_j . They satisfy that $\lambda_i = \Delta s \times 2^{i+1}$ and $\lambda_j = \Delta s \times 2^{j+1}$ in the extended tetralet transform, Δs is the sampling interval.

In ISO 4287, surface components including roughness, waviness and form are distinguished by the cutoff wavelengths λ_s , λ_c and λ_f respectively. That is to say, λ_s denotes the intersection between the even shorter wave components and the roughness, λ_c denotes the intersection between the roughness and waviness components and λ_f denotes the intersection between the waviness and form components.

As mentioned above, the HDM data only contains the 3D surface form and waviness information. Therefore, the surface component whose wavelength between λ_c and λ_f can be considered as the surface waviness and the rest is the surface form. Here, let $\lambda_1 = \lambda_c$ and $\lambda_j = \lambda_f$, where j is the designated level which depends on the defined cutoff wavelength λ_f . The recommended value of λ_f can be found in ISO 16610-29 [30], such as 2.5um, 8um, 25um, 80um, 250um, 0.8 mm, 2.5 mm, 8 mm, 25 mm and so on. The surface waviness $W(x, y)$ and form $F(x, y)$ can be obtained respectively as:

$$\begin{aligned} W(x, y) &= M_{1,j} = M_1 - M_j \\ &= \tilde{a}_{j-1} + \tilde{a}_{j-2} + \dots + \tilde{a}_1 \quad (j > 1) \end{aligned} \quad (28)$$

$$\begin{aligned} F(x, y) &= M_1 - W(x, y) = M_j \\ &= \tilde{a}_j + \tilde{a}_j \\ &= \tilde{a}_{j-1} \quad (j > 1) \end{aligned} \quad (29)$$

where M_1 is the reconstructed original surface.

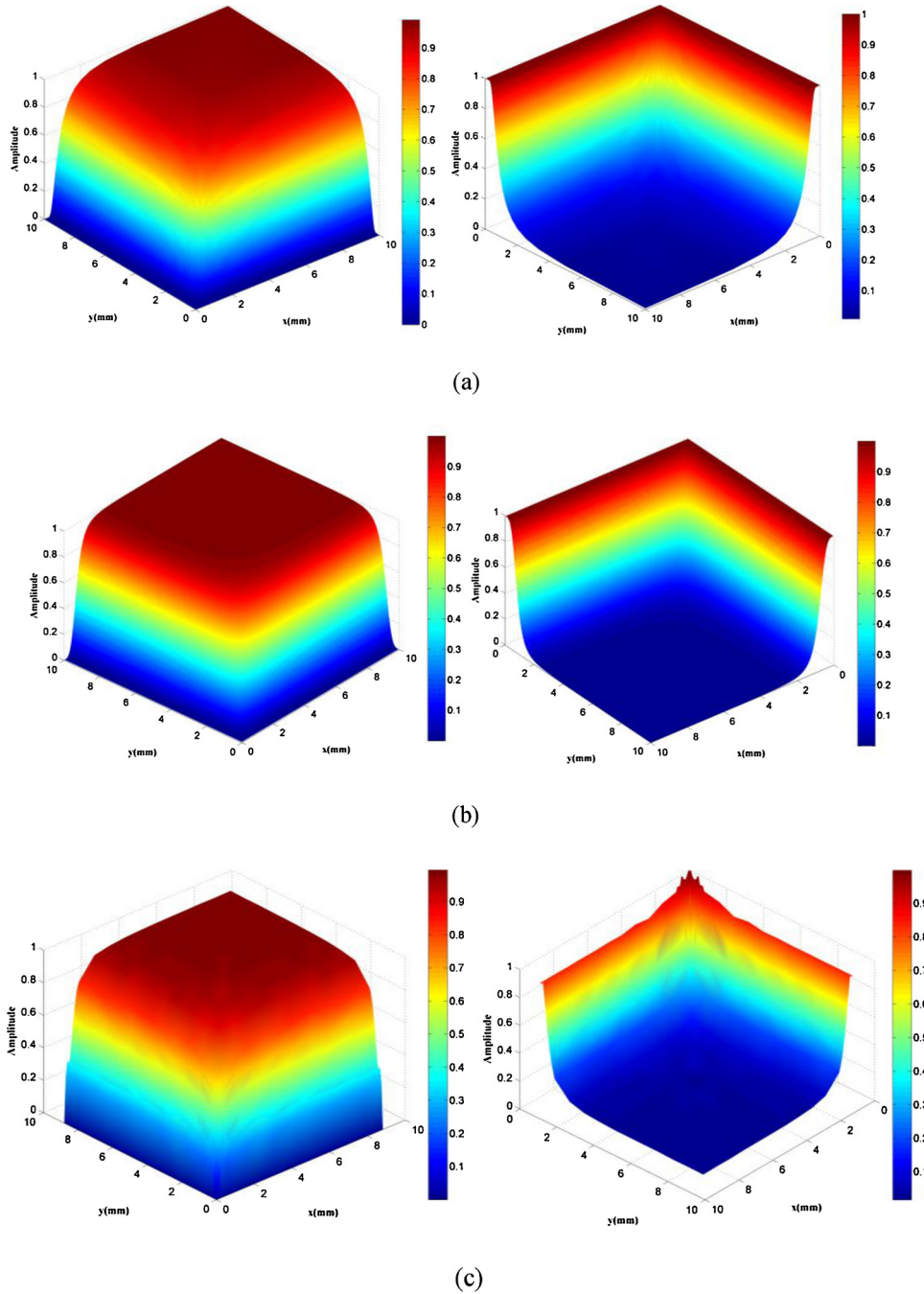


Fig. 9. (a) Amplitude transmission characteristics of areal Gaussian filter (b) Amplitude transmission characteristics of areal spline filter (c) Amplitude transmission characteristics of the extended tetrolet transform.

3.5. 3D characterization parameters of surface topography

More precisely, to verify the performance of the proposed filtering method, areal surface texture parameters are adopted to evaluate the filtering results. Profile parameters in surface characterization have already been defined by many different organizations and most of them have been written into standards. However, the adequate and reliable information of 3D surface topography cannot be provided by profile parameters, whereas the latter areal parameters may offer an attractive and realistic solution. Based on the latest areal surface texture standard ISO 25178-2 [31], several representative parameters including height parameters (S_q , S_p , S_v , S_z , S_d), shape parameters (S_{sk} , S_{ku}) and spatial parameters (S_{al} , S_{lr}) are selected.

(1) Height parameters

The root mean square height parameter S_q is defined as:

$$S_q = \sqrt{\frac{1}{A} \iint_A z^2(x, y) dx dy} \quad (30)$$

where A is a definition area and $z(x, y)$ is the height value of the surface at position x, y .

The maximum height parameter S_z is defined as:

$$S_z = S_p + S_v \quad (31)$$

where S_p is maximum peak height parameter and S_v is the maximum pit height parameter within the definition area A . The arithmetical mean height parameter S_a is defined as:

$$S_a = \frac{1}{A} \iint_A |z(x, y)| dx dy \quad (32)$$

(2) Shape parameters

The skewness of height distribution parameter S_{sk} is defined as:

$$S_{sk} = \frac{1}{S_q^3} \left[\frac{1}{A} \iint_A z^3(x, y) dx dy \right] \quad (33)$$

The kurtosis of height distribution parameter S_{ku} is defined as:

$$S_{ku} = \frac{1}{S_q^4} \left[\frac{1}{A} \iint_A z^4(x, y) dx dy \right] \quad (34)$$

(3) Spatial parameters

The spatial parameter S_{al} is the horizontal distance of $f_{ACF}(\tau_x, \tau_y)$ which has the fastest decay to η .

$$S_{al} = \min_{\tau_x, \tau_y \in R} \sqrt{\tau_x^2 + \tau_y^2} (R = \{(\tau_x, \tau_y): f_{ACF}(\tau_x, \tau_y) \leq \eta\}) \quad (35)$$

where $f_{ACF}(\tau_x, \tau_y)$ is the autocorrelation function and η is a specified constant with $\eta \in (0, 1)$. The default value is $\eta = 0.2$ in this paper. The surface texture aspect ratio parameter S_{tr} is defined as:

$$S_{tr} = \frac{\min_{\tau_x, \tau_y \in R} \sqrt{\tau_x^2 + \tau_y^2}}{\max_{\tau_x, \tau_y \in R} \sqrt{\tau_x^2 + \tau_y^2}} (R = \{(\tau_x, \tau_y): f_{ACF}(\tau_x, \tau_y) \leq \eta\}) \quad (36)$$

4. Numerical simulation

Gaussian filter [32] is the current standard filtering technique, and it is recommended in the ISO 16610-21 instead of 2RC filter. Nevertheless, Gaussian filter only can be applied in the continuous surface due to the obvious and fatal edge effect. Spline filter which can reduce the edge distortion has also been recommended in ISO 16610-22 [33]. Then they are expanded to areal Gaussian filter and areal spline filter for 3D surface [9,34]. By contrast, the proposed extended tetrolet transform can achieve a fine filtering solution both in the continuous and discontinuous surface. In order to show the strong efficiency of the proposed method, the three methods are compared in the aspects of filtering properties and filtering results.

4.1. Filtering properties

In order to facilitate the surface filtering properly, the extended tetrolet transform satisfies the following properties: (1) Finite Impulse Response (FIR), the tetromino support is finite, (2) linear phase, the small support and symmetry of tetrolet ensure that there will be no distortion in the filtered profiles, and (3) shape amplitude transmission, guarantees that a high-pass filter transmits almost all the wavelengths below a certain cut-off without attenuating its amplitude and heavily suppresses wavelengths above the cut-off and vice versa for the low-pass filter.

It is well known that a desirable filtering method should have a steep amplitude transmission curve near the cut-off wavelength [32–34]. The amplitude transmission curve indicates the filter transmits 50% at the cut-off wavelength. That is to say, a steeper amplitude transmission profile is preferred in surface filtering. The low-pass and high-pass amplitude transmission characteristics of areal Gaussian filter, areal spline filter and the extended tetrolet transform are illustrated in Fig. 9. The cut-off wavelengths in x and y directions are both set to 0.8 mm. For further comparison, the one dimensional low-pass amplitude transmission characteristics of the three filters are shown in Fig. 10. It is clear that the amplitude transmission profile of the extended tetrolet transform are steepest among the three filters, which demonstrates that the extended tetrolet transform can separate out surface topography features effectively.

4.2. Filtering results

A simulated continuous surface is generated by the equation of. It is clear that the cosine term can be considered as the surface waviness and the rest term is the surface form. The sampling interval is 0.2 mm in x and y directions, and the size of the simulated surface is 51.2mm × 51.2mm. The number of sampling points is 256 × 256 and the wavelength of the surface waviness is 6.4 mm. The continuous surface is shown in Fig. 11(a). In comparison, the discontinuous surface is obtained by getting rid of parts from the continuous surface which is shown in Fig. 11(b).

For the two simulated surfaces, areal Gaussian filter, areal spline filter and the extended tetrolet transform are applied to separate the form and waviness. The cutoff wavelength λ_f for areal Gaussian filter and areal spline filter is 25 mm, that is $\lambda_f = 25\text{mm}$. For the extended tetrolet transform, the corresponding wavelength cutoff is $\lambda_f = 0.2 \times 2^{6+1} = 25.6\text{mm}$ (close to 25 mm) with the decomposition level $i = 6$. Therefore, the waviness is $W(x, y) = M_{1,6} = M_1 - M_6 = \tilde{a}_5 + \tilde{a}_4 + \tilde{a}_3 + \tilde{a}_2 + \tilde{a}_1$ and the form is $F(x, y) = M_1 - W(x, y) = M_6 = \tilde{a}_6 + \tilde{a}_6 = \tilde{a}_5$. Fig. 12 shows the filtered results of the continuous and discontinuous surface using areal Gaussian filter, and Fig. 13 shows the filtered results of the continuous and discontinuous surface using areal spline filter. Moreover, the corresponding filtered results of the continuous and discontinuous surface

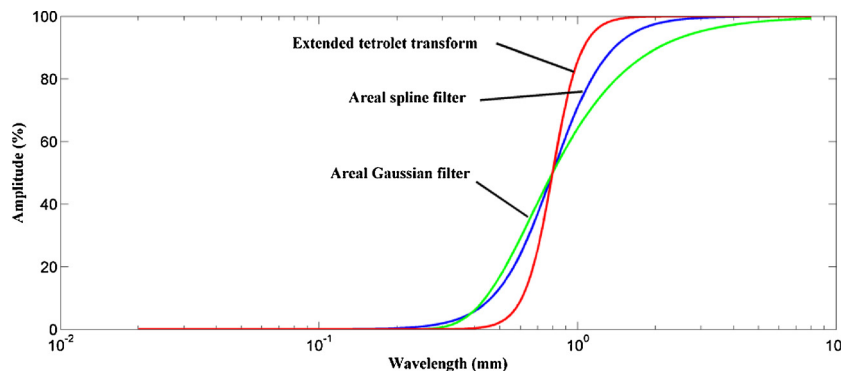


Fig. 10. Low-pass amplitude transmission characteristics of the three filters.

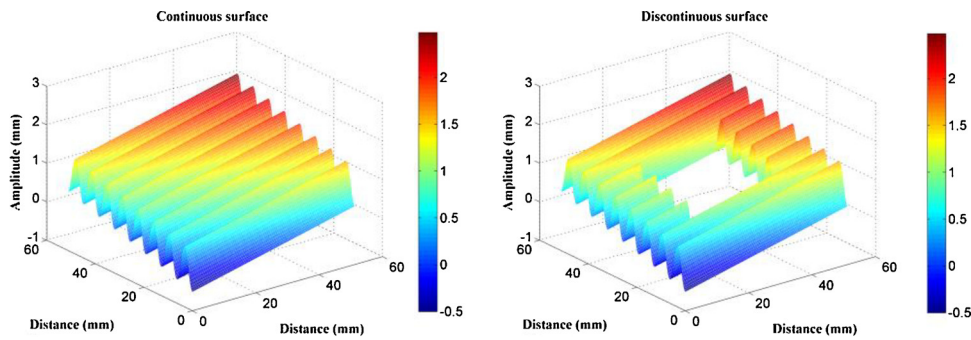


Fig. 11. (a) Continuous surface (b) Discontinuous surface.

using the extended tetrolet transform are illustrated in Fig. 14. In Fig. 12, whatever the continuous surface or discontinuous surface, edge distortions are evident in the results of areal Gaussian filter at the boundary and the hole. Therefore, to eliminate the edge effects and evaluate the surface parameters, half a cutoff wavelength is discarded at the beginning and the end of the surface when using areal Gaussian filter [34]. According to ISO 16610-21 and 16610-61 [32,34], the cutoff areal Gaussian filtered results of the continuous surface can be considered as the standard filtered results, which is shown in Fig. 15(a).

With standard filtered results as references, for the continuous surface, it is clear that form and waviness of areal spline filter and the extended tetrolet transform are both similar to the cutoff areal Gaussian filtered results (see Figs. 13(a), 14 (a) and 15 (a)). However, for the discontinuous surface, a big difference has emerged in these filtered results. In the areal Gaussian filtering, the obvious edge distortion exists both at the boundary and the hole. After discarding the end effect, the cutoff areal Gaussian filtered results of the discontinuous surface is too few to meet the parameter evaluation requirement, which is shown in

Fig. 15(b). In the areal spline filtering, the end effect which is reduced in the boundary still occurs beside the holes (see Fig. 13(b)), but it rarely exists in the extended tetrolet transform (see Fig. 14(b)). To be specific, the form and waviness are distorted greatly beside the holes by areal Gaussian filter and areal spline filter, but the surface components are still separated accurately by the extended tetrolet transform.

Furthermore, 3D characterization parameters described in Section 3.5 are calculated to evaluate the filtered surface components quantitatively. As the cutoff areal Gaussian filtered results of the continuous surface are considered as the standard filtered results, the standard values of waviness parameters are calculated in Table 1. According to ISO 25178-2 [31], all the filtered waviness should meet the parameter evaluation requirement that parameters are calculated in a definition area whose length of side is twice long-cutoff wavelength of waviness. But for the discontinuous surface, the definition area of the cutoff areal Gaussian filtered results is too few to evaluate the parameters. Meanwhile, the discontinuous surface is obtained by getting rid of parts from the continuous surface, which won't change the parameter value in the

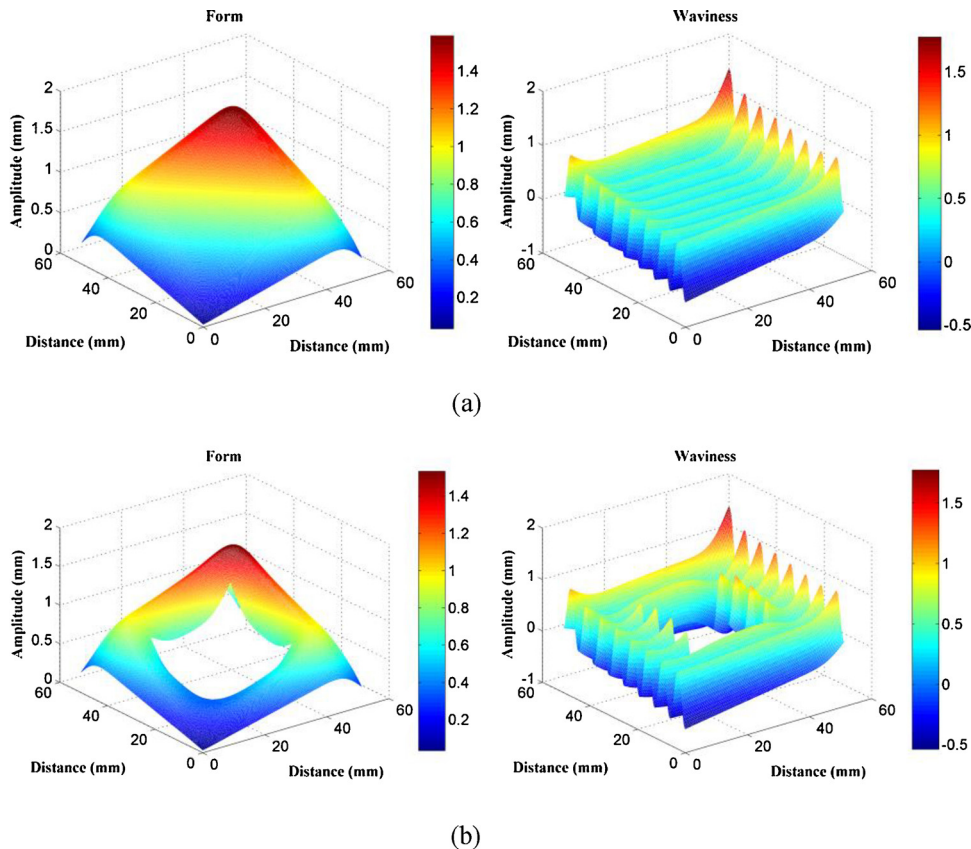


Fig. 12. Results of areal Gaussian filter (a) Continuous surface (b) Discontinuous surface.

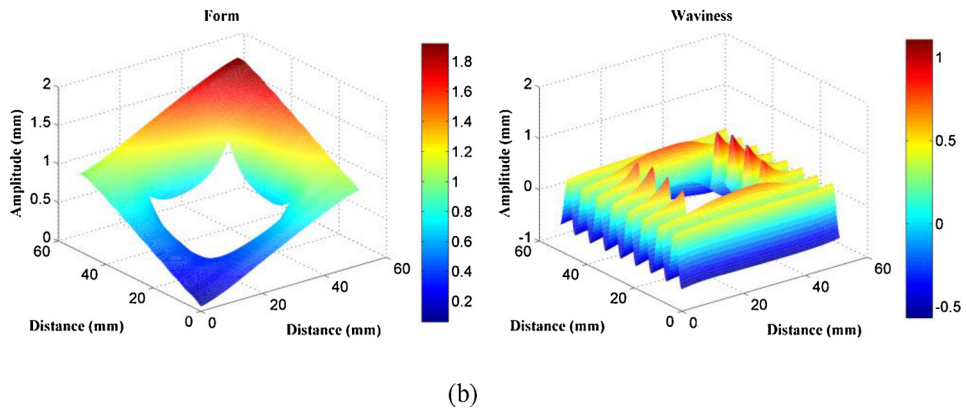
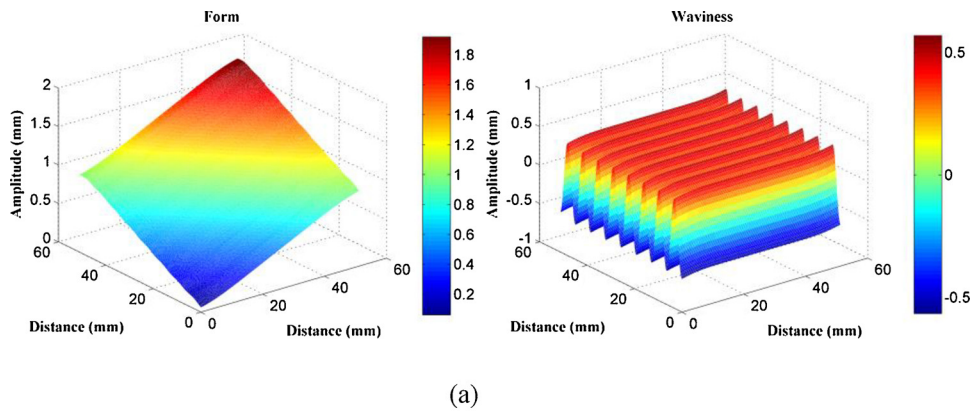


Fig. 13. Results of areal spline filter (a) Continuous surface (b) Discontinuous surface.

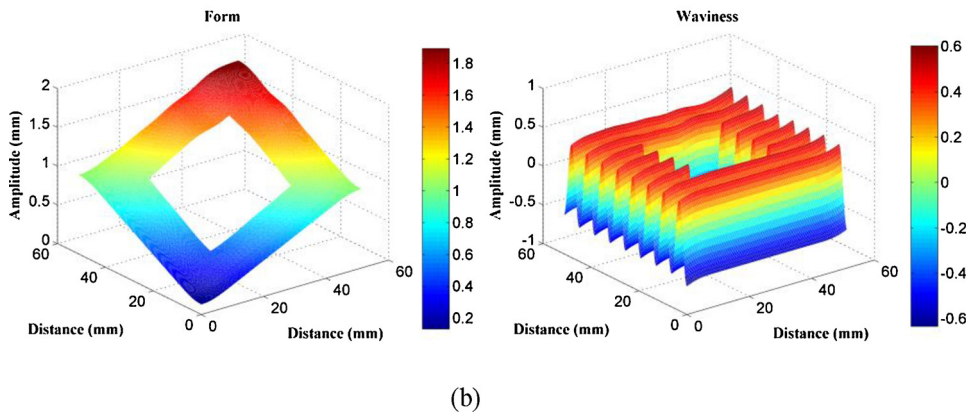
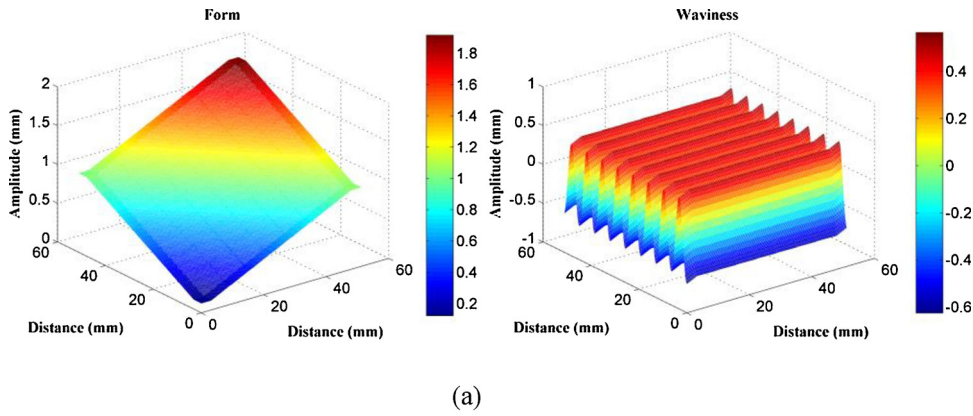


Fig. 14. Results of the extended tetrolet transform (a) Continuous surface (b) Discontinuous surface.

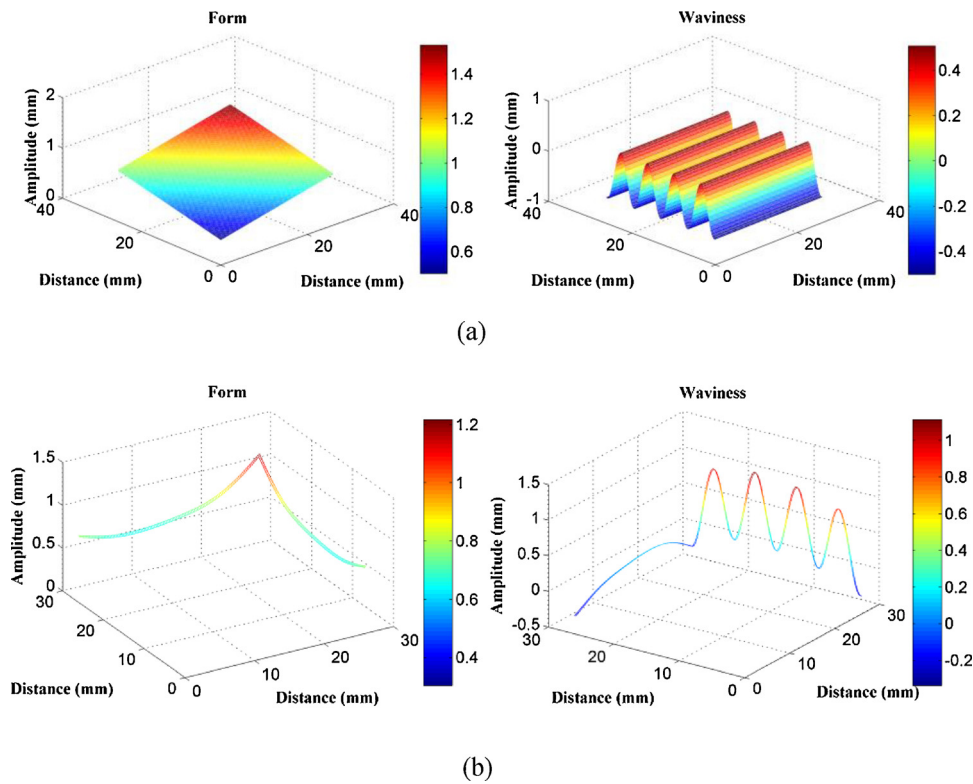


Fig. 15. Results of cutoff areal Gaussian filter (a) Continuous surface (b) Discontinuous surface.

Table 1
The standard values of waviness parameters.

The cutoff areal Gaussian filtered results of the continuous surface					
S_q /mm	0.357	S_p /mm	0.520	S_v /mm	0.484
S_z /mm	1.004	S_a /mm	0.322	S_{sk}	0.066
S_{ku}	1.493	S_{al}	7.066	S_r	0.220

Table 2
The comparisons of the waviness parameters in the continuous surface.

Simulation	Continuous surface		Diff ₁	Diff ₂
	Areal spline	Extended tetralet		
S_q /mm	0.354	0.357	-1.02%	0.04%
S_p /mm	0.528	0.524	1.52%	0.71%
S_v /mm	0.491	0.485	1.45%	0.33%
S_z /mm	1.019	1.009	1.44%	0.48%
S_a /mm	0.319	0.323	-1.03%	0.04%
S_{sk}	0.066	0.066	-0.36%	-0.20%
S_{ku}	1.494	1.492	0.08%	-0.02%
S_{al}	7.073	7.071	0.10%	0.07%
S_r	0.222	0.221	0.81%	0.26%

certain definition area. Therefore, both for the continuous surface and discontinuous surface, waviness parameters of the cutoff areal Gaussian filtered results of the continuous surface are the basis values. The comparisons of the waviness parameters using areal spline filter and extended tetralet transform in the continuous and discontinuous surface are listed in Tables 2 and 3. The differences are calculated as:

$$Diff_1 = \frac{\text{par}(\text{areal spline filter}) - \text{par}(\text{cutoff areal Gaussian filter})}{\text{par}(\text{cutoff areal Gaussian filter})} \quad (37)$$

Table 3
The comparisons of the waviness parameters in the discontinuous surface.

Simulation	Discontinuous surface		Diff ₁	Diff ₂
	Areal spline	Extended tetralet		
S_q /mm	0.464	0.358	29.98%	0.15%
S_p /mm	0.786	0.547	51.24%	5.14%
S_v /mm	0.585	0.513	20.96%	6.08%
S_z /mm	1.371	1.060	36.59%	5.54%
S_a /mm	0.422	0.325	30.79%	0.78%
S_{sk}	0.092	0.063	38.25%	-4.88%
S_{ku}	1.991	1.497	33.40%	0.29%
S_{al}	8.711	7.073	23.28%	0.10%
S_r	0.279	0.222	26.57%	0.81%

$$Diff_2 = \frac{\text{par}(\text{extended tetralet transform}) - \text{par}(\text{cutoff areal Gaussian filter})}{\text{par}(\text{cutoff areal Gaussian filter})} \quad (38)$$

where Diff₁ and Diff₂ denote the deviations of the filtered results by areal spline filter and extended tetralet transform respectively, and par(•) means the corresponding surface parameters.

Here, a small deviation of 10% is tolerated, which can be considered as no edge distortions. From Table 2, the differences of the waviness parameters for the continuous surface among cutoff areal Gaussian filter, areal spline filter and the extended tetralet transform are within 2%, which indicates the three filtering methods are suitable for the continuous surface. As for the discontinuous surface in Table 3, the deviations of waviness parameters obtained from the discontinuous surfaces are over 20% for the areal spline filter, but within 7% for the extended tetralet transform. Hence, it can infer that the proposed extended tetralet transform is suitable to separate the components for the

Table 4
Correlation coefficient of the continuous surface.

$r(F_{c,Standard}, F_{c,Spline})$	0.9999	$r(F_{c,Standard}, F_{c,Tetrolet})$	1.000
$r(W_{c,Standard}, W_{c,Spline})$	0.9999	$r(W_{c,Standard}, W_{c,Tetrolet})$	1.000

Table 5
Correlation coefficient of the discontinuous surface.

$r(F_{disc,Spline}, F_{disc,Spline})$	0.9622	$r(F_{disc,Tetrolet}, F_{disc,Tetrolet})$	0.9994
$r(W_{disc,Spline}, W_{disc,Spline})$	0.9418	$r(W_{disc,Tetrolet}, W_{disc,Tetrolet})$	0.9990

discontinuous surface without edge distortions.

In order to further evaluate the similarity among these surface components filtered by the above three filter methods, the Pearson's correlation coefficient r is used [35,36]. It is calculated as:

$$r(X, Y) = \frac{Cov(X, Y)}{\sqrt{Var(X)Var(Y)}} = \frac{\sum_m \sum_n (X_{mn} - \bar{X})(Y_{mn} - \bar{Y})}{\sqrt{(\sum_m \sum_n (X_{mn} - \bar{X})^2)(\sum_m \sum_n (Y_{mn} - \bar{Y})^2)}} \quad (39)$$

where X and Y are two matrices with the size of $m \times n$, \bar{X} and \bar{Y} are the corresponding mean values of the two matrices. Obviously, the correlation coefficient $r \in [0, 1]$, and the closer this value is to 1, the similarity is better. Table 4 shows the correlation between the different filter methods, $F_{c,Standard}$, $F_{c,Spline}$, $F_{c,Tetrolet}$ and $W_{c,Standard}$, $W_{c,Spline}$, $W_{c,Tetrolet}$ denote the filtered form and waviness of the continuous surface by cutoff areal Gaussian filter, areal spline and extended tetrolet transform respectively. Table 5 shows the correlation between the filtered results of the continuous surface and discontinuous surface, $F_{disc,Spline}$, $F_{disc,Tetrolet}$ and $W_{disc,Spline}$, $W_{disc,Tetrolet}$ denote the filtered form and waviness of the discontinuous surface by cutoff areal Gaussian filter, areal spline and extended tetrolet transform respectively. From Tables 4 and 5, the very strong correlation further indicates the applicability of the extended tetrolet transform in the discontinuous surface filtering.

5. Case study

5.1. Case study I

A steel groove plate which can be considered as a discontinuous surface with deep edges is shown in Fig. 16. The measured plate surface

is shown in Fig. 16(a), and the converted gray image is shown in Fig. 16(b). The computational time of the extended tetrolet transform depends on the size of HDM data of the part. Considering the computational efficiency and the square scope of the extended tetrolet transform, a piece of square surfaces is randomly selected from the plate, as shown in Fig. 16(b).

The size of the selected surface is 51.2mm \times 51.2mm, and the sampling interval is 0.2 mm. The number of sampling points is 256 both in X and Y direction. With the roughness and waviness specification $Ra = 1.6\mu m$, $Rz = 6.3\mu m$, and $Wt = 2\mu m$, the cutoff wavelengths of roughness are 0.08 mm and 0.8 mm, the cutoff wavelengths of waviness are 0.8 mm and 8 mm, respectively [37]. As the HDM data only contains the 3D surface form and waviness information, the cutoff wavelength $\lambda_f = 8mm$. For the extended tetrolet transform, the corresponding cutoff wavelength is $\lambda_f = 0.2 \times 2^{4+1} = 6.4mm$ (close to 8 mm) with the decomposition level $i = 4$. Therefore, the waviness is $W(x, y) = M_{1,4} = M_1 - M_4 = \tilde{a}_3 + \tilde{a}_2 + \tilde{a}_1$ and the form is $F(x, y) = M_1 - W(x, y) = M_4 = \tilde{a}_4 + \tilde{a}_4 = \tilde{a}_3$. There are about 0.07 million points in the selected part, and the computational time is 8.6 s. The filtering results are listed in Fig. 17. It is clear that the form and waviness are separated completely, there are no distortion at the boundary and the deep edges. From the exactly filtered waviness, it can be seen that the surface quality is acceptable, and it indicates the machining process is steady and no surface irregularities occur.

5.2. Case study II

The second case study is based on a top surface of engine cylinder block which is illustrated in Fig. 18(a). The material of the engine cylinder block is Cast iron FC250. This surface is a major sealing surface in automotive powertrain and it is manufactured by rough milling, semi-finish milling and finish milling. The milling process was carried out on an EX-CELL-O machining center using a face milling cutter which has a diameter of 200 mm with 15 cutting inserts intercalated by 3 wiper inserts. Quaker 370 KLG cutting fluid was used. The milling speed was 816.4 m/min, the depth of milling was 0.5 mm, and feed rate was 3360 mm/min. With the limitation of the measurement range, the entire top surface is divided into two parts (up and down) averagely for measuring. Then the measuring results of the two parts can be stitched through the measurement system. The whole measuring result is similar to Fig. 1 and the converted gray image is shown in Fig. 18(b).

The size of each part of the top surface both are 102.4mm \times 102.4mm, and the sampling interval is 0.2 mm. The number of sampling points is 512 both in X and Y direction. With the roughness and waviness specification $Ra = 3.2\mu m$, $Rz = 12.5\mu m$, and $Wt = 10\mu m$, the cutoff wavelengths of waviness are 2.5 mm and 25 mm [37]. The corresponding

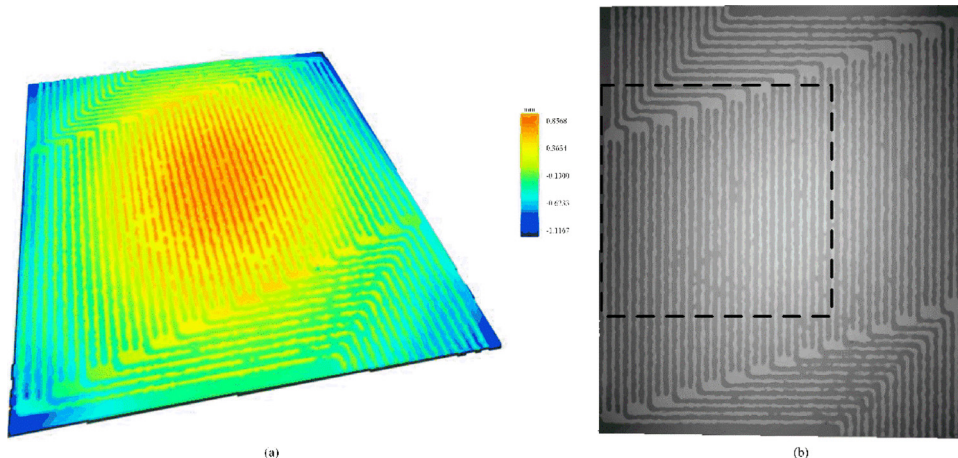


Fig. 16. Discontinuous surface (a) Steel plate surface (b) The converted gray image.

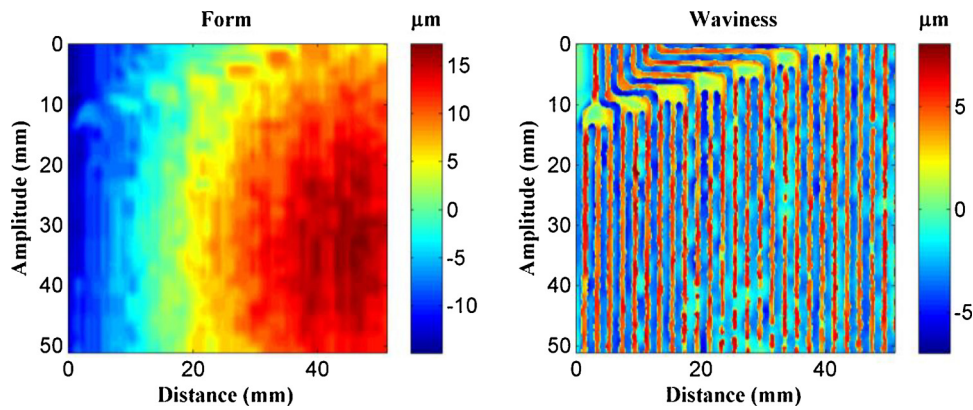


Fig. 17. Plate surface in 2D view.

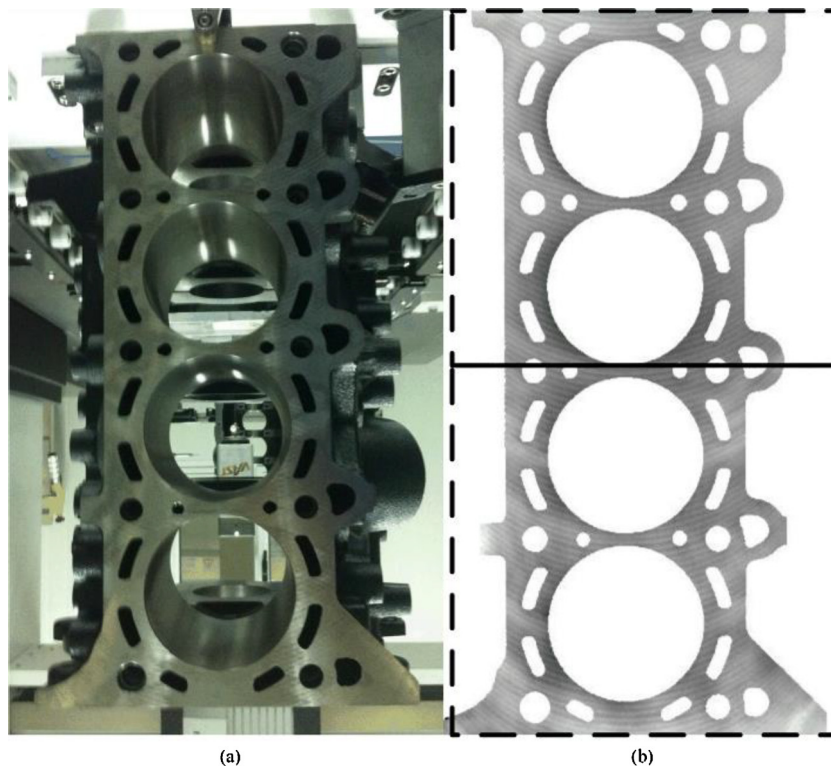


Fig. 18. Discontinuous surface (a) Top surface of engine cylinder block (b) The converted gray image.

cutoff wavelength is $\lambda_f = 0.2 \times 2^{6+1} = 25.6\text{mm}$ (close to 25 mm) with the decomposition level $i = 6$. Similarly, the waviness is considered as $W(x, y) = \tilde{a}_5 + \tilde{a}_4 + \tilde{a}_3 + \tilde{a}_2 + \tilde{a}_1$ and the form is $F(x, y) = \tilde{a}_6 + \tilde{a}_6 = \tilde{a}_5$. There are about 0.3 million points in each part, and the computational time is 31.6 s. The filtered results are visualized in Fig. 19. It can be seen that the tooling marks of the surface are totally separated from the surface form, and there is also no distortion at the boundary and the holes. The exactly filtered results indicate the surface quality is acceptable and the machining process is steady.

Leakage is always a serious concern in engine manufacturing, and it may lead to engine overheating, compression loss and power reduction. Typically, leakage occurs most in the interface between engine cylinder block and head. In this surface, form and roughness can be tolerated by the conformability of the gasket material. However, the waviness with peak-to-peak variation cannot be tolerated and may lead to highly localized contact and leakage [6]. As a consequence, the waviness

separated from the top surface of engine cylinder block using the proposed filtering method can indicate the possible leakage area.

Another top surface of engine cylinder block is illustrated in Fig. 20. The block has passed the leakage test, but the leakage still existed. The tooling marks of the surface are obtained using the extended tetrolet transform, and the waviness parameters of 8 positions in Fig. 20 are listed in Table 6.

It is clear that the waviness parameters of position 4 and 5 are abnormal. Furthermore, the magnified images of the two positions are shown in Fig. 21. The red and blue alternating color represents the tooling marks with the largest peak-to-peak variation. The possibility of leakage is function of the peak-to-peak values of the tooling marks. This implies that position 4 and 5 may be the leakage area, and the leakage will most likely occur in position 4. Thus, to obtain the susceptibility to leakage, evaluation of the exactly filtered waviness at critical areas is necessary. Above all, the extended tetrolet transform can make good applications in the field of the 3D discontinuous surface filtering.

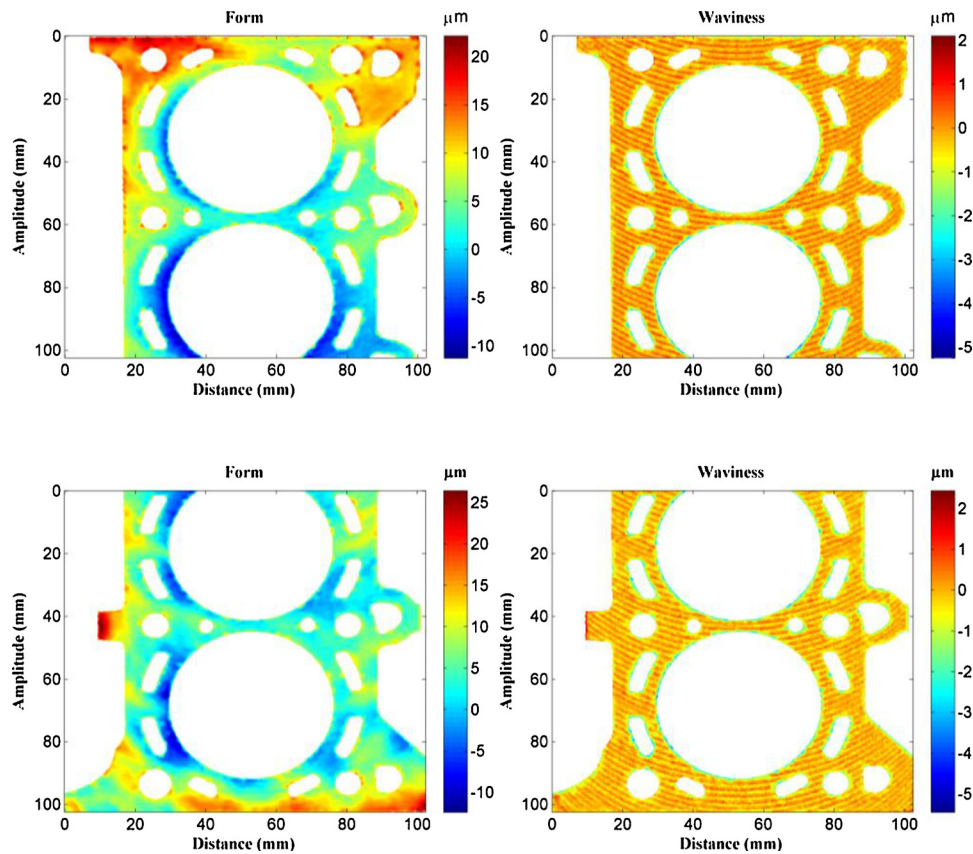


Fig. 19. Top surface of engine cylinder block.

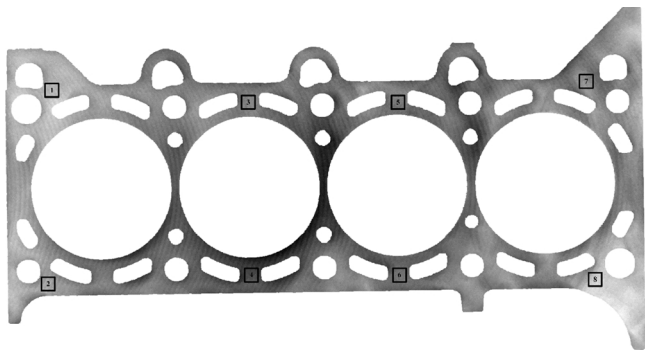


Fig. 20. Leakage surface.

6. Discussion

With high requirements of surface quality, surface components such as form, waviness and roughness for the precise work-pieces are

required strictly to guarantee quality. The boundaries and holes in the discontinuous engineering surface are crucial positions which contain vast surface information, and they have a great impact on various kinds of factors such as tools, marks, vibrations, warping strains and heat treatment during the machining process. Extracting the exact surface components by surface filtering has played an essential role in analyzing the manufacturing process and functional behaviors. As for these discontinuous engineering surfaces, the proposed filtering method which overcomes the drawback of edge effect that occurs in the discontinuous surface using traditional filtering methods is necessary.

Some improved aspects of the proposed method are listed as follow:

- 1) Due to small support, symmetry, orthogonality and adaptive geometrical structure, the proposed method can solve the line and surface singularities in the 3D discontinuous surface which causes edge distortions.
- 2) The proposed method develops an edge detector to identify the surface boundaries and holes in advance so that different forms of decomposition are applied.

Table 6

Waviness parameters of each position.

Position	1	2	3	4	5	6	7	8
$S_q/\mu\text{m}$	0.764	0.974	0.979	3.256	1.156	1.005	0.837	0.669
$S_p/\mu\text{m}$	2.926	3.222	2.894	7.619	4.672	3.348	3.058	2.439
$S_v/\mu\text{m}$	2.749	3.228	5.191	13.634	5.861	4.221	2.519	2.460
$S_z/\mu\text{m}$	5.675	6.450	8.085	21.254	10.533	7.569	5.578	4.898
$S_a/\mu\text{m}$	0.597	0.762	0.736	2.150	0.792	0.708	0.651	0.527
S_{sk}	0.085	-0.040	-0.544	-1.325	-1.156	-0.158	0.397	-0.096
S_{ku}	3.392	3.212	4.786	5.78	7.202	5.077	3.641	3.423
S_{al}	3.606	4.123	4.123	4.123	4.123	4.123	4.123	4.123
S_{tr}	0.806	0.825	0.972	0.206	0.294	1.144	0.922	0.972

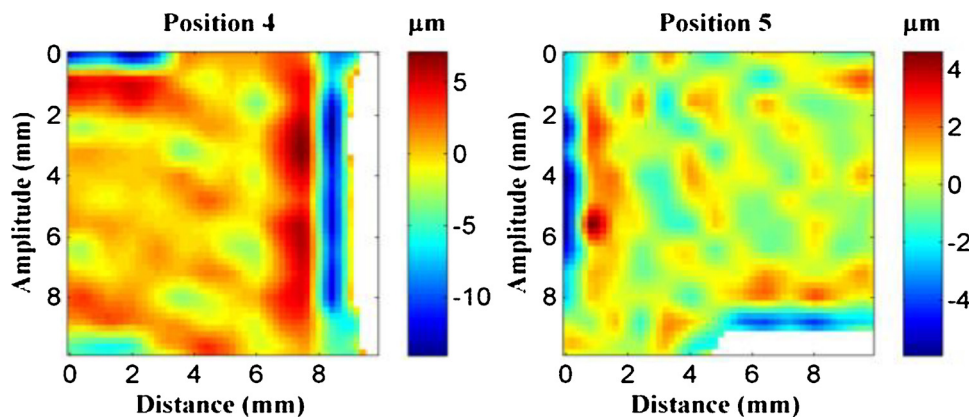


Fig. 21. (a) Waviness of position 4 (b) Waviness of position 5.

- 3) The proposed method can well extract the decomposed and reconstructed subsurface which represent different surface components.

Nevertheless, little block effect occurs in the extended tetrolet transform due to the constitution of tetrominoes, some smooth techniques are expected to optimize the proposed method further in future. Once the exact surface components are obtained, it can diagnose the internal causes of surface flaws so that to find the product defect in time. Moreover, it can indicate surface irregularities so that engineers can adjust the manufacturing process quickly to avoid the unqualified work-pieces entering into the next costly machining or assembling stage. However, there have been only a few attempts to exploit the relationship between surface components and the functional behavior of the part, which is the next research topic.

7. Conclusions

In this paper, a new filtering method based on the extended tetrolet transform is proposed which focuses on the 3D discontinuous surface topography. The proposed method consists of 3D discontinuous surface measurement and point cloud conversion, edge detector generation, extended tetrolet transform and 3D characterization parameters evaluation. Meanwhile, a comprehensive comparison with areal Gaussian filter and areal spline filter, the proposed filtering method is validated to do well in 3D surface filtering without edge distortion, especially for the discontinuous surface. Simulated and experimental discontinuous surfaces demonstrate that the proposed method can be a powerful tool for 3D discontinuous surface filtering. Moreover, 3D surface parameters can be calculated based on the filtered surface, which indicates the surface quality and functional performance. Additionally, considering the effectiveness of the extended tetrolet transform, it is expected to be superior to the current ISO standardized Gaussian filter and spline filter. The proposed filtering method can be a powerful tool in 3D discontinuous surface topography analysis in the future, when more and more discontinuous engineering surfaces need to be analyzed.

Acknowledgements

This work was supported by the National Natural Science Foundation of China (Grant No. 51535007 and 51775343). All experiments were performed at SAIC GM Wuling Automobile (SGMW), we are grateful to SGMW engineers for their experimental support.

References

- [1] Ramasamy SK, Raja J. Performance evaluation of multi-scale data fusion methods for surface metrology domain. *J Manuf Syst* 2013;32:514–22.
- [2] ISO 4287. Geometrical product specifications (GPS)-surface texture: profile method: terms, definitions and surface texture parameters. 1997.
- [3] Bhuiyan MSH, Choudhury IA, Dahari M. Monitoring the tool wear, surface roughness and chip formation occurrences using multiple sensors in turning. *J Manuf Syst* 2014;33:476–87.
- [4] Haruyama S, Nurhadiyanto D, Choiran MA, Kaminishi K. Influence of surface roughness on leakage of new metal gasket. *Int J Press Vessels Pip* 2013;111–112:146–54.
- [5] Ledoux Y, Lasseux D, Favreliere H, Samper S, Grandjean J. On the dependence of static flat seal efficiency to surface defects. *Int J Press Vessels Pip* 2011;88:518–29.
- [6] Malburg MC. Surface profile analysis for conformable interfaces. *J Manuf Sci Eng* 2003;125:624.
- [7] Bottiglione F, Carbone G, Mangialardi L, Mantriota G. Leakage mechanism in flat seals. *J Appl Phys* 2009;106:104902.
- [8] Bottiglione F, Carbone G, Mantriota G. Fluid leakage in seals: an approach based on percolation theory. *Tribol Int* 2009;42:731–7.
- [9] Hanada H, Saito T, Hasegawa M, Yanagi K. Sophisticated filtration technique for 3D surface topography data of rectangular area. *Wear* 2008;264:422–7.
- [10] Tomonori G, Kazuhisa Y. An optimal discrete operator for the two-dimensional spline filter. *Meas Sci Technol* 2009;20:125105.
- [11] Fu S, Muralikrishnan B, Raja J. Engineering surface analysis with different wavelet bases. *J Manuf Sci Eng* 2003;125:844.
- [12] Jiang XQ, Blunt L, Stout KJ. Development of a lifting wavelet representation for surface characterization. *Proc. R. Soc. A* 2000;456:2283–313.
- [13] Raja J, Muralikrishnan B, Fu S. Recent advances in separation of roughness, waviness and form. *Precision Eng* 2002;26:222–35.
- [14] Huang Z, Shih AJ, Ni J. Laser interferometry hologram registration for Three-dimensional precision measurements. *J Manuf Sci Eng* 2006;128:1006.
- [15] Wang M, Xi L, Du S. 3D surface form error evaluation using high definition metrology. *Precision Eng* 2014;38:230–6.
- [16] Du S, Liu C, Huang D. A shearlet-based separation method of 3D engineering surface using high definition metrology. *Precision Eng* 2015;40:55–73.
- [17] Du S, Liu T, Huang D, Li G. A fast and adaptive bi-dimensional empirical mode decomposition approach for filtering of workpiece surfaces using high definition metrology. *J Manuf Syst* 2018;46:247–63.
- [18] Du S, Huang D, Wang H. An adaptive support vector machine-based workpiece surface classification system using high-definition metrology. *IEEE Trans Instrum Meas* 2015;64(10):2590–604.
- [19] Du S, Liu C, Xi L. A selective multiclass support vector machine ensemble classifier for engineering surface classification using High definition metrology. *J Manuf Sci Eng* 2014;137:011003.
- [20] Shao Y, Du S, Xi L. 3D machined surface topography forecasting with space-time multioutput support vector regression using High definition metrology. *Proceedings of the ASME 2017 International DesignEngineering Technical Conferences & Computers and Information inEngineering Conference*. 2017.
- [21] Wang M, Ken T, Du S, Xi L. Tool wear monitoring of wiper inserts in multi-insert face milling using three-dimensional surface form indicators. *J Manuf Sci Eng* 2015;137:031006.
- [22] Nguyen HT, Wang H, Hu SJ. Characterization of cutting force induced surface shape variation in face milling using High-definition Metrology1. *J Manuf Sci Eng* 2013;135:041014.

- [23] Nguyen HT, Wang H, Tai BL, Ren J, Jack Hu S, Shih A. High-definition metrology enabled surface variation control by cutting load Balancing I. *J Manuf Sci Eng* 2015;138:021010.
- [24] Shao Y, Yin Y, Du S, Xia T, Xi L. Leakage monitoring in static sealing interface based on Three dimensional surface topography indicator. *J Manuf Sci Eng* 2018;140:101003–12.
- [25] Zhang M, Levina E, Djurdjanovic D, Ni J. Estimating distributions of surface parameters for classification purposes. *J Manuf Sci Eng* 2008;130:031010.
- [26] Liao Y, Stephenson DA, Ni J. Multiple-scale wavelet decomposition, 3D surface feature exaction and applications. *J Manuf Sci Eng* 2012;134:011005.
- [27] Krommweh J. Tetrolet transform: a new adaptive Haar wavelet algorithm for sparse image representation. *J Vis Commun Image Represent* 2010;21:364–74.
- [28] Krommweh J, Ma J. Tetrolet shrinkage with anisotropic total variation minimization for image approximation. *Signal Process* 2010;90:2529–39.
- [29] Golomb SW. *Polyominoes*. Princeton, NJ: Princeton University Press; 1994.
- [30] ISO 16610-29. Geometrical product specifications (GPS)-filtration part 29: linear profile filters: spline wavelets. 2015.
- [31] ISO 25178-2. Geometrical product specifications(GPS)-surface texture: areal - part 2: terms, definitions and surface texture parameters. 2012.
- [32] ISO 16610-21. Geometrical product specifications (GPS)-filtration part 21: linear profile filters: gaussian filters. 2015.
- [33] ISO 16610-22. Geometrical product specifications (GPS)-filtration part 22: linear profile filters: spline filters. 2015.
- [34] ISO 16610-61. Geometrical product specifications (GPS)-filtration part 61: linear areal filters: gaussian filters. 2015.
- [35] Karl Pearson FRS. I. Mathematical contributions to the theory of evolution. —VII. On the correlation of characters not quantitatively measurable. *Philos Trans R Soc Lond* 1900;195:1–405.
- [36] Pearson K. Notes on the history of correlation. *Biometrika* 1920;13:25–45.
- [37] ISO 4288. Geometrical product specifications (GPS)-surface texture: profile method: rules and procedures for the assessment of surface texture. 1996.